JCTC Journal of Chemical Theory and Computation

Article

pubs.acs.org/JCTC

Stalking Higher Energy Conformers on the Potential Energy Surface of Charged Species

Vincent Brites,[†] Alvaro Cimas,[†] Riccardo Spezia,[†] Nicolas Sieffert,[‡,∥] James M. Lisy,*[,⊥] and Marie-Pierre Gaigeot*[,†,§]

[†]LAMBE CNRS UMR8587, Université d'Evry val d'Essonne, Blvd F. Mitterrand, Bât Maupertuis, 91025 Evry, France

[‡]Université Grenoble Alpes, DCM, 38000 Grenoble, France

[∥]CNRS, DCM, 38000 Grenoble, France

[⊥]Department of Chemistry, University of Illinois at Urbana-Champaign, Urbana, Illinois 61801, United States

[§]Institut Universitaire de France, 103 Blvd St Michel, 75005 Paris, France

ABSTRACT: Combined theoretical DFT-MD and RRKM methodologies and experimental spectroscopic infrared predissociation (IRPD) strategies to map potential energy surfaces (PES) of complex ionic clusters are presented, providing lowest and high energy conformers, thresholds to isomerization, and cluster formation pathways. We believe this association not only represents a significant advance in the field of mapping minima and transition states on the PES but also directly measures dynamical pathways for the formation of structural conformers and isomers. Pathways are unraveled over picosecond (DFT-MD) and microsecond (RRKM) time scales while changing the amount of internal energy is experimentally achieved by changing the loss channel for the IRPD measurements, thus directly probing different kinetic and isomerization pathways. Demonstration is provided for $Li^+(H_2O)_{3,4}$ ionic clusters. Nonstatistical formation of these ionic clusters by both direct and cascade processes, involving isomerization processes that can lead to trapping of high energy conformers along the paths due to evaporative cooling, has been unraveled.

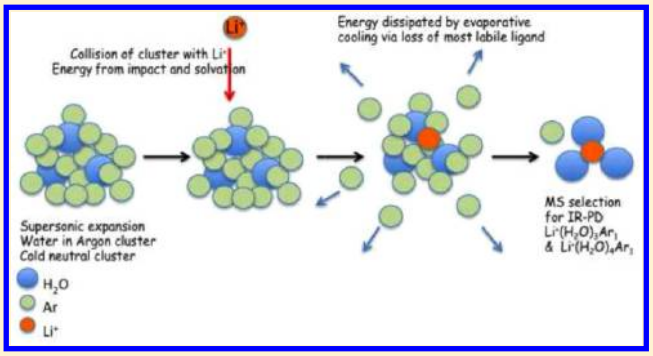

INTRODUCTION

While knowledge of the minima on a potential energy surface (PES) is essential for characterizing specific conformers and isomers of flexible biomolecules and molecular assemblies, the energy barriers separating the minima are of equal importance as they are keys for the dynamics of conformational isomerization. Vibrational spectroscopy is a very efficient experimental tool for structural information at the minima and has become a key component in double resonance and action spectroscopies to map out the barriers and pathways between various conformers. For gas-phase studies of molecules, molecular assemblies, and clusters, IRMPD (infrared multiphoton dissociation) and IRPD (infrared predissociation) experiments are now widely applied in various domains of chemistry, physics, and biology.[1−5] The paradigm in these experiments is that molecular beam expansion methods used to generate these species yield the lowest energy conformation, driven by kinetic and entropic effects. It is however nowadays more broadly accepted that the formation of molecules and complexes in supersonic expansions does not always follow thermodynamic control and that kinetically trapped conformations can be formed even under cold thermodynamic conditions.

Kinetic trapping on potential surfaces has been observed in a wide variety of systems using a variety of experimental and theoretical methods. Using a molecular beam discharge source, Duncan and co-workers have obtained the acetyl cation and protonated ketene; the latter is 196 kJ/mol higher in energy, with a barrier of over 200 kJ/mol from the lower energy acetyl cation.[6] When attaching sodium atoms to cold water clusters in a molecular beam pick-up source, high energy conformers of $Na(H_2O)_3$ were identified, through the use of photoionization and beam expansion conditions that allowed selective detection of different conformers.[7] Conformers of alkali metal atoms complexed to cytosine, formed in an ion flow tube source, were generated by collisional cooling.[8] The higher energy conformers exhibited different threshold behavior for collision-induced dissociation, and the experimental dissociation energies did not necessarily correspond to the global ground state on the potential energy surface.[8] In larger systems, a theoretical study of the self-assembly of ligated metal clusters, $M_{12}L_{24}$, indicated the involvement of kinetically trapped structures of smaller sizes,[9] and the trapping behavior was sensitive to the bend angle of the ligands and the metal−ligand binding strength. The

Received: September 9, 2014
Published: February 4, 2015

DOI: 10.1021/ct5008197
J. Chem. Theory Comput. 2015, 11, 871−883

binding of phosphate ion to the phosphate ion binding protein was modeled using Transition Path Theory, where the trapping kinetics were found to depend on the nature of the charged sites on the surface of the protein both near and distant to the binding site.[10] The mechanical manipulation and imaging of virus particles by atomic force microscopy was used to identify kinetic intermediates predicted by simulations of assembly and/or disassembly.[11]

Of direct relevance to the present work, a number of gas-phase investigations are bearing on the dynamics of conformational isomerization and kinetic trapping. Conformational distributions of bradykinin have been studied by Rizzo and co-workers,[12] showing the appearance of high energy conformers. Clemmer and Russell et al. have conducted studies to bridge the gap between solution and the gas phase with a detailed study of the structural evolution of a undecapeptide, in the final stages of an electrospray ionization source.[13] Here the compact configuration of the peptide, present in solution, is retained in the gas phase, in both hydrated and (following evaporative cooling by loss of water) dehydrated forms. Collisional activation of the trapped conformer was needed to generate the more stable elongated form. Subsequent experiments, using site-directed mutagenesis, established the stabilizing role of polar side chains of glutamine and phenylalanine with the charge centers, enabling the compact form to be trapped in the gas phase.[14] Additional experimental examples can be found in the review by Zehnacker.[15]

Several IRPD argon-tagging experiments performed in our group have also demonstrated that high energy conformers of singly charged clusters are kinetically trapped.[16−18] Our explicit goal is to extend to charged systems spectroscopic methodologies that have already been shown capable to map out barriers and conformational pathways in neutral species, as pioneered by Zwier and co-workers.[19,20] Using laser methods to prepare and induce conformational changes, they were able to directly map the PES of flexible neutral biomolecules, with precise control of the energy deposited in the molecular system. Johnson and co-workers have elegantly approached the study of multiple conformers in cluster ions, using IR-IR pump and probe techniques combined with mass spectrometry, but do not directly address relative energetics.[21]

There is no theoretical foundation providing a detailed microscopic explanation on the mechanistic processes that lead to such kinetic trapping. In order to understand how the mechanistic and thermodynamic conditions in the experiments can lead to the production of higher energy conformers, we combine different time scale theoretical approaches. Our goal is not only to provide a detailed microscopic understanding of the processes at play but also to attempt to rationalize the experimental approach (vide infra) and apply it more broadly and more systematically for mapping potential energy surfaces of complex ionic systems, i.e., directly providing minima, transition states, and dynamical pathways for the formation of structural isomers.

We combine DFT-based molecular dynamics simulations (DFT-MD) and RRKM kinetics calculations. The dynamics will provide a detailed mechanistic comprehension of the cluster's formation, dynamics of conformational isomerization, and possible kinetic trapping into higher energy conformers. The dynamics mirror the specific experimental nonequilibrium thermodynamic conditions, i.e., collisional processes and evaporative cooling. The kinetic calculations will provide conformational isomerization at longer time-scales. Our simulations are aimed at not only characterizing energy landscapes[22] but also sorting out the most significant ingredients that decide the conformation adopted by charged clusters, including thermodynamic and entropic effects, dynamics, and kinetics, in a direct way.

The theoretical investigation presented here is related to the experiments from the Lisy group,[16,23,24] where both structural and energetic aspects of different conformations are obtained, in practice by changing the observed loss channel for the spectroscopic IRPD measurements, which enables us to sample species with varying amounts of internal (kinetic and potential) energy. This variation is a result of the collisional and evaporative cooling formation process in the experimental setup, explained below and shown schematically in Figure 1.

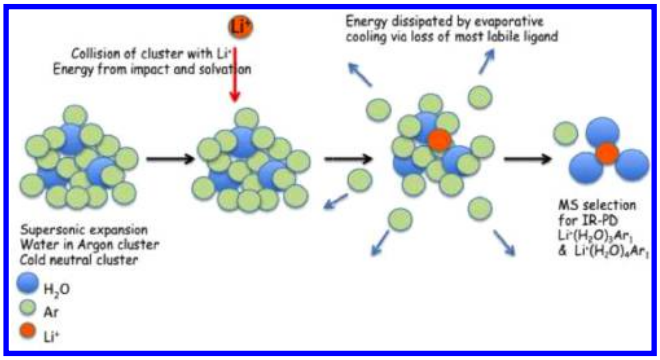

Figure 1. Illustration of our IRPD experimental setup with an emphasis on the evaporative cooling process that is investigated in the present theoretical work.

The experiment indeed deserves some description in order to estimate the challenges to be addressed by the theoretical simulations. The present work is specifically dedicated to kinetic trapping of $Li^+(H_2O)_{3,4}$ clusters.

As illustrated in Figure 1, neutral clusters are formed via a supersonic expansion of argon and water. Lithium ions are produced via thermionic emission and collide perpendicularly with the fully expanded neutral clusters approximately 3 cm downstream from the nozzle. The nascent cluster ions contain an excess of internal energy (~10 eV, ~965 kJ/mol) from the collisional and solvation processes that is dissipated through evaporative cooling of the most labile ligands. The internal energy of the cluster ions depends on the composition of the neutral clusters formed after the initial expansion (Ar:H_2O ratio), and the neutral clusters contain a significant number of argon atoms. These cluster ions will stabilize primarily through the evaporative loss of argon atoms. For this process, the ion approaches the neutral cluster embedded in argon, with excess energy rapidly dissipated by argon evaporation. If sufficient argon is present, the cluster ions will retain one argon atom (or more) and will necessarily have a lower internal energy (or effective temperature), compared to cluster ions formed primarily through the evaporative loss of water.[25] The lower internal energy makes it possible for the ion to bind to the neutral cluster with little or no rearrangement to the original configuration of its molecular constituents formed in the supersonic expansion. Often, this particular cluster ion configuration is not the global minimum-energy structure. If the barrier to rearrangement leading to a lower energy configuration exceeds the binding energy of argon in the cluster ion, one can kinetically trap higher energy cluster ion configurations that would not be expected to be thermody-

DOI: 10.1021/ct5008197
J. Chem. Theory Comput. 2015, 11, 871−883

namically present at low (~50−150 K) temperatures. By combining a tandem quadrupole mass spectrometer, IRPD spectra of mass-selected parent ions can be obtained by detecting the loss of one or more neutral constituents of the parent ion.

We take here the typical example of IRPD vibrational spectroscopy of $Li^+(H_2O)_{3,4}$ clusters which has been investigated by the Lisy group in the past[23,24] and has been recently revisited by the group.[16] In this latest work, the existence of higher energy conformers has been demonstrated through IRPD spectroscopy. The variables associated with the IRPD spectra are the presence and number of argon atoms attached, the specific fragmentation channel (e.g., loss of argon or loss of multiple species), and the IR spectroscopic signatures. The amount of internal energy present can vary from a few kJ/mol of kinetic energy to over 40 kJ/mol of potential energy (from high energy conformers on the ground PES). Depending on the cluster internal energy, different kinetic and isomerization pathways can be probed.

In the molecular dynamics simulations that are performed in the present theoretical work, by focusing on how Li^+ approaches the water cluster, varying the trajectory, impact parameter, and kinetic energy (effective temperature), the critical factors involved in the formation of specific $Li^+(H_2O)_{3,4}$ conformers will be unraveled. A similar methodology was used to consider the collision between a metal atom and a metal cluster.[26] Fragmentation and scattering could be grouped into two broad groups: instantaneous fragmentation and a process mediated by successive rearrangements. Fragmentation occurred for low-impact parameter collisions. However, for larger impact parameters, the energy is spread throughout the system, allowing it to sample other configurations.

In our theoretical study, questions addressed are how the mechanistic and thermodynamic conditions typical of the experiments possibly influence the final conformer formed, how trapping of high energy conformers is achieved, over what time-scale, and what is the internal energy (temperature) of the final clusters formed in the experimental setup. The present work provides a robust combined experimental and theoretical state-of-the art tool that we trust can be readily applied to more complex molecular systems (typically involving biological molecules).

We describe below the theoretical approaches used in our work (Theoretical Methods section), and our results are presented in terms of the potential energy surface of $Li^+(H_2O)_{3,4}$ clusters, dynamical nonstatistical formation of the clusters, temperature effects on the kinetic trapping of higher energy conformers, short-time and long-time scale dynamics, and kinetics. A direct estimation of the temperature of the clusters as they form in the experiment is also presented and discussed. We finish this paper with our perspectives on the synergy between the theoretical approaches presented here and the experiment.

THEORETICAL METHODS

State-of-the art theoretical computational chemistry methods have been combined: PES (potential energy surface) determination, i.e., minima and transition states, using DFT, MP2, and CCSD(T) electronic levels, DFT-based molecular dynamics simulations (DFT-MD), metadynamics (biased DFT-MD), and RRKM statistical kinetic theory. These methods are organized as follows. The PES describes conformers, relative energies, and energy barriers, and RRKM provides rate constants and time-scales for conformational isomerization, within the statistical approximation of the theory. Metadynamics helped characterize transition state domains, for subsequent transition state geometry optimizations. DFT-MD of the collisions between Li^+ and the water cluster provides the mechanistic and nonstatistical aspects of $Li^+(H_2O)_n$ clusters formation, conformational isomerization along the cluster formation process, and trapping into higher energy wells, over a few picoseconds time-scale.

Potential Energy Surface Characterization. The static electronic structure calculations for the PES characterization of $Li^+(H_2O)_{3,4}$ clusters have been performed with Gaussian 09.[27] The equilibrium geometries and harmonic frequencies of the $Li^+(H_2O)_{3,4}$ conformers have been obtained at the MP2 level of theory.[28] The aug-cc-pVTZ basis sets[29] have been employed for the description of hydrogen and oxygen atoms, and the aug-cc-pCVTZ basis set[30] was chosen for the description of lithium. Gibbs free energies were calculated at 100 K. For reference calculations at a higher level of theory, single point CCSD(T)[31] energies have been obtained on the MP2 optimized structures. The associated CCSD(T) Gibbs free energies at 100 K have been obtained by adding the thermal corrections computed at the MP2 level to the single point CCSD(T) energies. Supplementary DFT single point calculations have been performed on the MP2 optimized structures in order to check the accuracy of the electronic representation and setup (i.e., DFT functional, pseudopotentials, mixed Gaussian and plane-wave basis set, cubic box dimension) of the DFT-MD dynamics. See section DFT-MD Simulations in Theoretical Methods for the details of the DFT-MD simulations and setup within the CP2K package.[32]

DFT-MD Simulations. DFT-based Born−Oppenheimer molecular dynamics simulations have been performed with the CP2K package,[32,33] where the nuclei are treated classically and the electrons quantum mechanically within the DFT (density functional theory) formalism. BLYP[34,35] including the Grimme D2 correction for dispersion,[36] combined with Goedecker−Teter−Hutter (GTH) pseudopotentials[37,38] is used. Note that electrostatic interactions are the leading terms for the structures and energetics of charged clusters of interest here. A hybrid Gaussian and plane wave representation of the electronic wave function is employed with the aug-QZV2P Gaussian basis set (QZV2P for lithium) and a plane-wave density cutoff of 450 Ry. A cubic cell with a side of 24 $Å^3$ was chosen, and the time-step was 0.4 fs. Choices of the Gaussian basis set and the plane-wave energy cutoff were carefully determined through convergence tests with respect to these parameters for $Li^+(H_2O)_{3,4}$ optimized clusters, checking that the relative energies between the conformers obtained with all electron calculations and the CP2K setup are consistent. See the presentation and discussion of these results in section Potential Energy Surface Characterization in Theoretical Methods.

On top of the usual way to choose the size of the cubic cell in order to accommodate the cationic systems of interest, the box size is dictated here by the simulated collisional process where the lithium cation is thrown toward the water cluster target from a long enough distance where it does not interact with the water cluster. The decoupling technique of Martyna and Tuckerman[39] has been applied in order to eliminate the effect of the periodic images of the charge density, so as to simulate gas phase processes. The final choice made of the 24 Å cubic box length is necessary in order to ensure there are no

DOI: 10.1021/ct5008197
J. Chem. Theory Comput. 2015, 11, 871−883

electrostatic issues from the decoupling technique. We have indeed carefully checked this box length with energy convergence tests. For three different initial configurations of the Li^+ collision with the $(H_2O)_4$ water cluster, i.e., Li^+ arriving toward the water cluster from above (case 1, $\theta = 0°$ in Figure 2), from a diagonal of the cubic box (case 2, $\theta = 45°$ in Figure 2), or from a location roughly within the water plane (case 3, $\theta = 90°$ in Figure 2), always keeping the ion at a distance of 7 Å from the water center of mass (as explained in DFT-MD Protocol for the Collisions below), we have calculated the energy of these configurations for cubic box lengths of 20, 24, 26, 28, and 30 Å. From 24 to 30 Å, the electronic energy of the configurations fluctuate from 0.8 kJ/mol (case 1) to a maximum of 3.1 kJ/mol (case 2). This is within the accuracy of the electronic method employed and shows that the 24 Å cubic box length is more than acceptable for the dynamics performed here for the collisions. Note also that a box length of 16 Å is enough to fulfill the requirements of energy convergence if one is interested in the optimized conformers of $Li^+(H_2O)_{3,4}$ clusters.

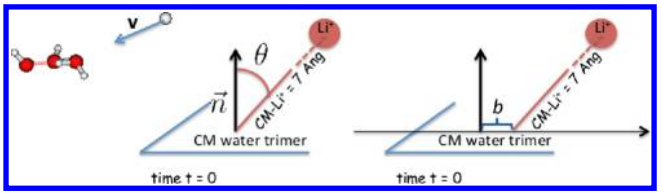

Figure 2. Schematic views of the initial conditions ($t = 0$) for the collision between Li^+ and a water cluster. Left: general illustration ($(H_2O)_3$ for the picture). Middle: illustration of the angle θ used in Figure 8: the initial impact angle between Li^+ and the water cluster, defined with respect to the normal of the plane containing the three (or four) oxygen atoms of the water cluster: $\theta = 0° \rightarrow Li^+$ initially located at the vertical of the plane, $\theta = 90° \rightarrow Li^+$ initially positioned within the plane. Right: illustration of the measure of the impact parameter b.

Metadynamics for Transition State Regions. Metadynamics biased DFT-based molecular dynamics simulations[40,41] have been performed using CP2K and the same settings described in section DFT-MD Simulations in Theoretical methods. Two collective variables were used: the coordination of the Li^+ cation with respect to the oxygen atoms of the water molecules and the dipole moment of the water cluster calculated with the TIP3P classical model of water.[42] Gaussian functions were added periodically every 40 fs of dynamics. Analysis of the free energy profiles extracted from the metadynamics simulations and of the associated trajectories clearly reveal isomerization between the conformers, as will be discussed in due course in the Results section. Beyond the knowledge of free energy profiles, metadynamics simulations were used to characterize the transition state (TS) regions between conformers of $Li^+(H_2O)_{3,4}$ clusters, i.e., TS structures and energetics. The energetics are especially relevant for our purpose of investigating the possible kinetic trapping of conformers. Transition state searches were done with the Gaussian package[27] at the reference MP2 level of representation previously discussed. Geometries were extracted from the metadynamics trajectories in the regions of the free energy surface corresponding to transition between isomers and were used as starting points for geometry optimizations of TS. These TSs will be presented and discussed in the section Results.

The coordination number (CN) of Li^+ used as one metavariable is calculated with the following formula:

$$\mathrm{CN}(Li^+, \mathrm{OW}) = \sum_{i=1,3} \frac{1 - \left(\frac{d_i(Li^+ - \mathrm{OW}_i)}{2.80}\right)^{15}}{1 - \left(\frac{d_i(Li^+ - \mathrm{OW}_i)}{2.80}\right)^{30}} \quad (1)$$

where OW represents an oxygen atom from any of the three water molecules and $d_i(Li^+ - \mathrm{OW}_i)$ is the distance between Li^+ and the oxygen OW_i of water molecule number i (in Å). This is the standard general definition used in CP2K for metadynamics biased MD simulations. We have checked that with this formula, the coordination numbers of Li^+ are exactly equal to the expected values (1 to 4) in the different optimized structures of $Li^+(H_2O)_{3,4}$ presented in Figure 3. The value of 2.80 in the formula has been adjusted on the $Li^+\cdots H_2O$ complex in order to separate the two situations, i.e., ion

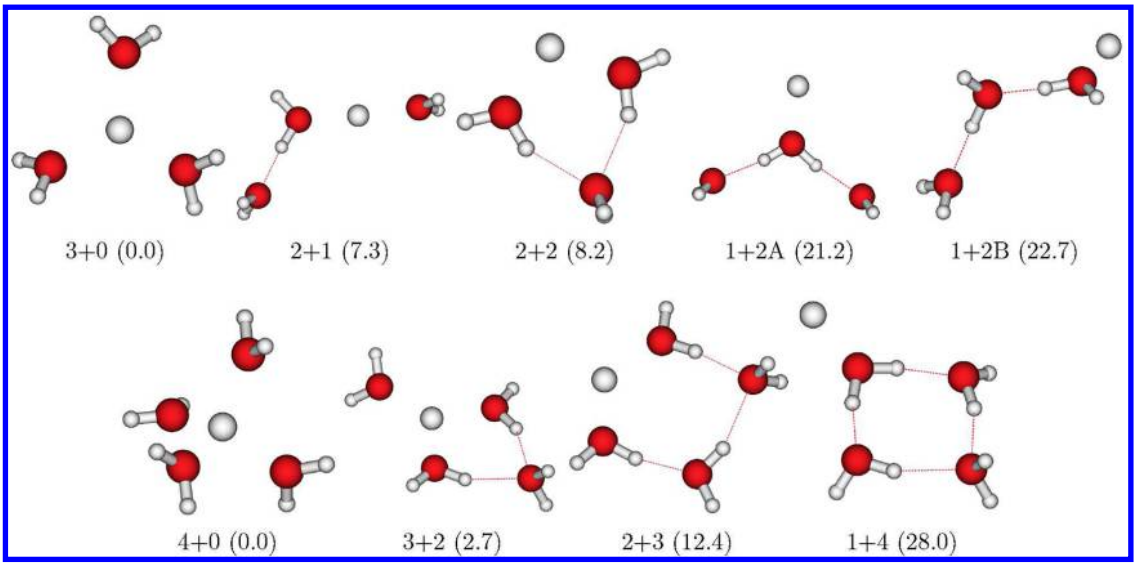

Figure 3. Optimized structures of $Li^+(H_2O)_3$ (top) and $Li^+(H_2O)_4$ (bottom) at the MP2 level; Gibbs free energy differences at 100 K in parentheses (kcal/mol). See text for the labeling "X+Y" of the conformers.

DOI: 10.1021/ct5008197
J. Chem. Theory Comput. 2015, 11, 871−883

coordinated to water (CN = 1) and ion not coordinated to the water molecule (CN = 0). The 15 and 30 values in the exponents are typical of these functions. The final CN(Li^+,OW) function is a sigmoidal curve with a midpoint at 2.80 Å and width of 1.00 Å.

DFT-MD Protocol for the Collisions. A scheme to illustrate the collision setup is presented in Figure 2. Initial (time t = 0 of the dynamics) positions and velocities for Li^+ colliding with $(H_2O)_{3,4}$ clusters were generated following the well-established protocol from Hase et al.,[43,44] that we have applied in previous investigations of chemical reactivity by collisions, modeling collision induced dissociations (CID).[45,46] Initial structures for the water clusters are the lower energy conformers, and the initial atomic velocities were chosen by adding a quasi-classical Boltzmann distribution of vibrational/rotational energies at a given temperature T. The targeted temperature corresponds to the experimentally estimated temperature of the clusters formed by evaporative cooling of argon prior to the IRPD process:[23,24] ~50−150 K for argonated $M^+(H_2O)_nAr$ clusters and ~200−300 K for non-argonated $M^+(H_2O)_n$ clusters. Random orientations in Euler angles between the (rigid body) water cluster and the Li^+ ion are sampled in order to account for the random directions of the collisions between Li^+ and $(H_2O)_{3,4}$. Impact parameters (i.e., the distance between the cluster center of mass and the axis around which Euler angles are sampled) for the ion−water collision are set by random sampling between 0 and 1.8 Å ($(H_2O)_3$), 0−2.0 Å $(H_2O)_4$. The impact parameter maximum values are chosen according to the size of the water cluster. The initial distance between the Li^+ and the water cluster center of mass was set to 7 Å, a distance at which the ion/cluster interaction is negligible. A total of 70 initial conformations per system was chosen. This relatively low number of trajectories was dictated by the cost of DFT-MD but deemed sufficient (as will be demonstrated here) to acquire adequate statistics over the initial collisional parameters. One supplementary metric will be used in order to characterize the initial structures for collision (see Figure 2, middle): the initial impact angle between Li^+ and the water cluster, defined with respect to the normal of the plane containing the three (or four) oxygen atoms. An impact angle of 0° means that Li^+ is located at the vertical of the plane at time t = 0 of the collision, whereas 90° corresponds to Li^+ initially positioned within the plane.

As illustrated in Figure 1, in the experiment, as the Li^+ ion approaches the neutral water cluster embedded in argon, the excess kinetic energy is dissipated by evaporation of argon atoms. In our DFT-MD simulations of the collisional process, the explicit presence of the argon was not taken into account, as the number of argon atoms required would be computationally prohibitive at the DFT level. Instead a protocol for the dissipation of energy, mimicking the evaporative cooling of argons from the cluster ions in the experiment, has been applied in the simulations. This protocol for cooling by evaporation is supported by results from some of us from a classical simulation of cesium ions colliding with a neutral cluster of methanol[47] and is based on the following conclusions. For Cs^+ impacts less than 12 eV (1160 kJ/mol) in the lab frame, only evaporative cooling of the nascent cluster ions was observed, with the average evaporative loss of one methanol per cooling step. The evaporation process was rapid, with each loss reducing the rate of evaporation (and increasing the lifetime of the cluster ion). Lastly, the ion cluster lifetimes were remarkably uniform over a range of cluster ion sizes, over a wide range (~10 eV, ~965 kJ/mol) of collisional energies. These results show that the binding energy of the evaporating species determines the cluster ion lifetime, as excess internal energy is rapidly dissipated by evaporative cooling.

In the current DFT-MD simulations, argon evaporative cooling is much more facile and rapid due to the low binding energy of argon. However, the same behavior, as noted above in the evaporative cooling of the Cs^+−methanol cluster ions, is expected, where the hydrated Li^+ cluster ions stabilize through evaporation of the most labile ligand, in this case, argon. Over several successive evaporative events, the internal energy content of these cluster ions indeed decreases. Each evaporative step removes an amount of energy that is roughly equivalent to the argon···ion cluster interaction. In this model, the approach of the ion to the neutral water cluster is the mechanism that increases the kinetic/thermal energy. As the temperature of the system increases, some of the kinetic energy would be channeled into potential energy to eventually dissociate an argon atom from the clusters. This lowers the available kinetic energy remaining in the system and hence lowers the cluster temperature following the evaporative event. This is simulated here by a simple procedure of rescaling the velocities of the atoms. Along the collisional trajectory, all atom velocities are accordingly scaled down by an amount leading back to the targeted cluster temperature T, whenever T goes beyond $T+\Delta T$. Target temperatures in the DFT-MD collisions are based on the estimated temperatures from experiments[23,24] with ~50−150 K for $Li^+(H_2O)_nAr$ clusters. The same approach was used for the nonargonated cluster ions, with the higher binding energy of water resulting in effective temperatures of ~200−300 K for $Li^+(H_2O)_n$ clusters. ΔT is chosen at 40 and 60 K, respectively, for a target temperature of 100 and 300 K. With this procedure, the internal energy of the $Li^+(H_2O)_{3,4}$ cluster is thus decreased over time (as the collision proceeds), as in the experiment. In practice, we noted energy rescaling occurred during the first 500 fs of the collisional process with some 40−50 rescaling events for the low temperature (100 K) and over an even shorter time-scale of 200 fs at higher temperature (300 K) with less than 20 rescaling events.

For a given cluster temperature, 70 collisional trajectories are accumulated for statistical analyses. DFT-MD trajectories are accumulated for 1−2 ps. This dynamics time scale is just long enough to see the formation of $Li^+(H_2O)_{3,4}$ clusters and conformational isomerization processes between the higher energy conformers as will be shown and discussed in the Results section.

RRKM Kinetics. Collisional DFT-MD results are obtained over a 2 ps time-scale, while the clusters are experimentally entrained for about 100 μs up to the ion guide where they will be interrogated by the IR photon in the IRPD experiment. Longer time-scales are thus needed from the theoretical calculations. To achieve the 100 μs time scale dictated by the experimental setup before the IR interrogation, a time-scale obviously unreachable by DFT-MD simulations, we have employed the RRKM formalism within the framework of the statistical kinetic theories.[48] RRKM calculations were chosen in order to reach that time scale instead of classical MD simulations. Classical MD would have required validation of the force field (FF) used for $Li^+(H_2O)_n$ ionic clusters (i.e., the FF has to reproduce the ab initio relative energies between conformers and transition states), certainly needing reparameterization which we want to avoid. Furthermore, depending on the specific form of the force field, it might be that such

DOI: 10.1021/ct5008197
J. Chem. Theory Comput. 2015, 11, 871−883

Table 1. Relative Energies (kcal/mol) between the $Li^+(H_2O)_3$ Conformers[a]

	3+0	2+2	2+1	1+2A	1+2B	2+1−2+2	2+1−3+0	2+2−3+0	1+2A−2+1	1+2B−2+1
					energy					
MP2	0.0	6.7	7.5	20.8	22.5	8.3	8.6	8.5	21.4	22.9
CCSD(T)	0.0	6.9	7.8	21.4	23.2	8.6	8.9	8.6	21.9	23.5
BLYP-D2	0.0	6.7	7.3	22.0	23.0	8.3	8.5	7.9	22.6	23.1
$\Delta_{MP2-CCSD(T)}$	0.0	−0.2	−0.3	−0.6	−0.7	−0.3	−0.3	−0.1	−0.5	−0.6
$\Delta_{MP2-BLYP-D2}$	0.0	0.0	0.2	−1.2	−0.5	0.0	0.1	0.6	−1.2	−0.2
$\Delta_{CCSD(T)-BLYP-D2}$	0.0	0.2	0.5	−0.6	0.2	0.3	0.4	0.7	−0.7	0.4
Gibbs (100 K)										
MP2	0.0	8.2	7.3	21.2	22.7	8.8	8.1	9.0	21.6	23.2
CCSD(T)	0.0	8.4	7.7	21.7	23.4	9.1	8.4	9.1	22.1	23.8

[a]See text for all details. Notation: "*X*+*Y*" (e.g., 3+0) refers to optimized structures on the PES, and "*X*+*Y*−*Z*+*W*" refers to transition states between conformer "*X*+*Y*" and "*Z*+*W*".

Table 2. Relative Energies (kcal/mol) between the $Li^+(H_2O)_4$ Conformers[a]

	4+0	3+2	2+3	1+4	1+4−2+3	2+3−3+2	4+0−3+2
				Energy			
MP2	0.0	1.3	10.7	26.2	28.7	11.0	5.1
CCSD(T)	0.0	1.7	11.3	27.0	29.3	11.6	5.3
BLYP-D2	0.0	1.0	10.2	26.5	28.1	10.4	4.1
$\Delta_{MP2-CCSD(T)}$	0.0	−0.4	−0.6	−0.8	−0.6	−0.6	−0.2
$\Delta_{MP2-BLYP-D2}$	0.0	0.3	0.5	−0.3	0.6	0.6	1.0
$\Delta_{CCSD(T)-BLYP-D2}$	0.0	0.7	1.1	0.5	1.2	1.2	1.2
Gibbs (100 K)							
MP2	0.0	2.7	12.4	28.0	30.5	12.9	5.3
CCSD(T)	0.0	3.0	13.0	28.8	31.2	13.4	5.7

[a]See text for all details. Notation: "*X*+*Y*" (e.g., 4+0) refers to optimized structures on the PES, and "*X*+*Y*−*Z*+*W*" refers to transition states between conformer "*X*+*Y*" and "*Z*+*W*".

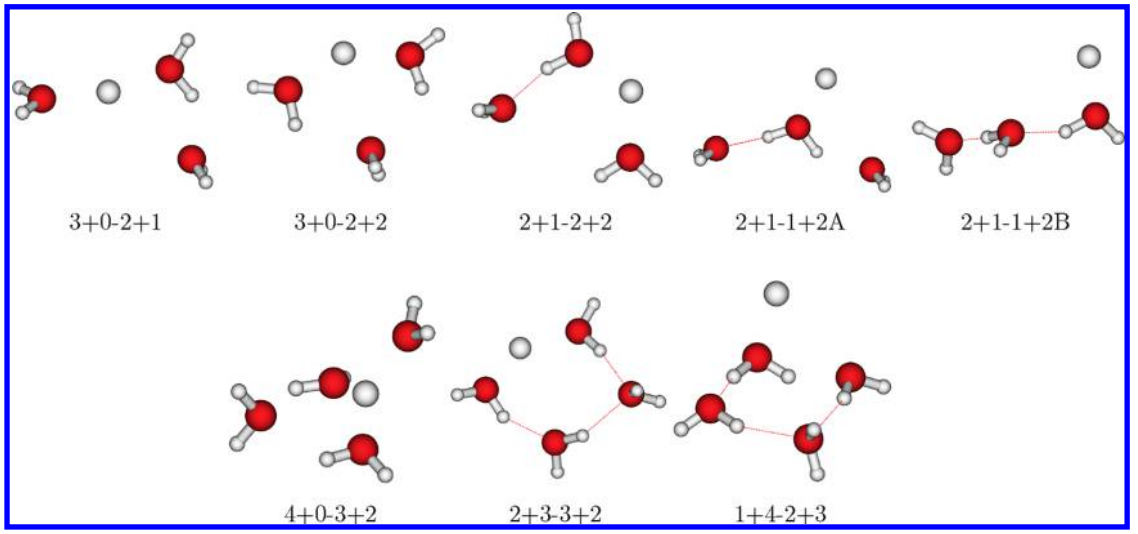

Figure 4. Optimized structures of the transition states of $Li^+(H_2O)_3$ (top) and $Li^+(H_2O)_4$ (bottom). The label of the TS is related to the names of the two stable structures connecting the TS (i.e., isomer1−isomer2, where isomer1(2) follows the labeling "*X*+*Y*" described in the text).

parametrization would not even be possible. RRKM was therefore the obvious choice in order to reach longer time-scales, as this method retains the ab initio electronic representation from the DFT-MD simulations.

Microcanonical rate coefficients have been calculated employing the usual equation of RRKM theory:[49]

$$k(E, J) = \sigma N^{\ddagger}(E, J)/h\rho(E, J) \quad (2)$$

where σ is the reaction symmetry factor and $N^{\ddagger}(E, J)$ and $\rho(E, J)$ are respectively the number of states at the transition state and the density of states at the minimum, both evaluated for an energy E and a total angular momentum J. The density and sum of states were determined employing the Forst algorithm[50] using the frequencies and moments of inertia determined from the MP2 ab initio calculations. The MP2 potential energy surface is identical to the BLYP-D2 one used for the trajectories; see previous discussion in section Potential Energy Surface Characterization in Theoretical Methods. The possibility of tunneling was accounted for in terms of a monodimensional probability according to the generalized

DOI: 10.1021/ct5008197
J. Chem. Theory Comput. 2015, 11, 871−883

Eckart potential.[51] Initial conditions of the RRKM calculations use the results from the DFT-MD trajectories, i.e., the knowledge of the population of isomers formed at the end of the 2 ps collision process and internal energy (temperature) of the clusters.

RESULTS

Potential Energy Surfaces of $Li^+(H_2O)_{3,4}$ Clusters. Figure 3 presents the lower energy conformers of $Li^+(H_2O)_{3,4}$ optimized at the MP2 level. The relative electronic and Gibbs free energies between the conformers are listed in Tables 1 and 2, respectively, for $Li^+(H_2O)_3$ and $Li^+(H_2O)_4$ clusters, for the different levels of electronic representations tested here. Structures are labeled *X*+*Y*, with *X* representing the coordination of Li^+ with respect to the oxygen atoms and *Y* the number of hydrogen bonds between water molecules.

All electronic levels of representation tested (BLYP-D2, MP2, CCSD(T)) provide the same PES (minima and transition states, see discussion below) to within ∼1 kcal/mol. Comparisons between these relative energies show that the BLYP-D2 representation used in the DFT-MD dynamics remarkably reproduces the MP2 and CCSD(T) relative energies, within a maximum error of 1.2 kcal/mol and within an average deviation of about 0.5 kcal/mol for all minima and transition states. There is in particular no energy reordering of the isomers. Gibbs free energies calculated at 100 K essentially provide the same relative energy order: only the relative energy of conformers 2+2 ($Li^+(H_2O)_3$) and 3+2 ($Li^+(H_2O)_4$) are slightly increased by 1.5 kcal/mol when entropy is taken into account. In the case of $Li^+(H_2O)_3$, this leads to an inversion in the relative order between conformers 2+2 and 2+1 (less than 1 kcal/mol of energy difference whether free or electronic energies are considered).

The optimized structures of transition states calculated at the MP2 level of theory are presented in Figure 4 for $Li^+(H_2O)_{3,4}$, and their energies are reported in Tables 1 and 2. Some of the initial geometries used for the transition state searches were extracted from the metadynamics simulations (DFT-MD representation) and related free energy profiles. The free energy profiles are presented in Figure 5 for $Li^+(H_2O)_3$ (top) and $Li^+(H_2O)_4$ (bottom). The metadynamics simulations were restricted to the conformational domain between the lower energy conformers of the clusters, i.e., 3+0 and 2+1/2+2 for $Li^+(H_2O)_3$ and 4+0 and 3+2 for $Li^+(H_2O)_4$. The free energy profiles show the energetics associated with the above-mentioned isomers of $Li^+(H_2O)_{3,4}$ and provide the free energy barriers between these conformers. One typically observes a ∼7−8 kcal/mol energy barrier for 3+0 → 2+1 (or 2+2) isomerization and a ∼4−5 kcal/mol energy barrier for 4+0 → 3+2 isomerization. The optimized structures at the transition states shown in Figure 4 at the MP2 electronic level and schematically placed in energy in Figures 6 and 7 essentially provide the same energetics as given by free energies.

Schemes of the potential energy surfaces are given in Figures 6 and 7. With these schemes, one can observe the energies of the barriers between conformational isomers and the possible opened pathways connecting these isomers. One can in particular see several pathways leading to conformer 2+1 from higher energy conformers on the potential energy surface of $Li^+(H_2O)_3$ and the small energy barrier of ∼1 kcal/mol to overcome from isomer 2+1 to the global minimum 3+0. Note also the direct opened path between 2+2 and 3+0 isomers with a barrier of ∼2 kcal/mol for the 2+2 → 3+0 isomerization. Very

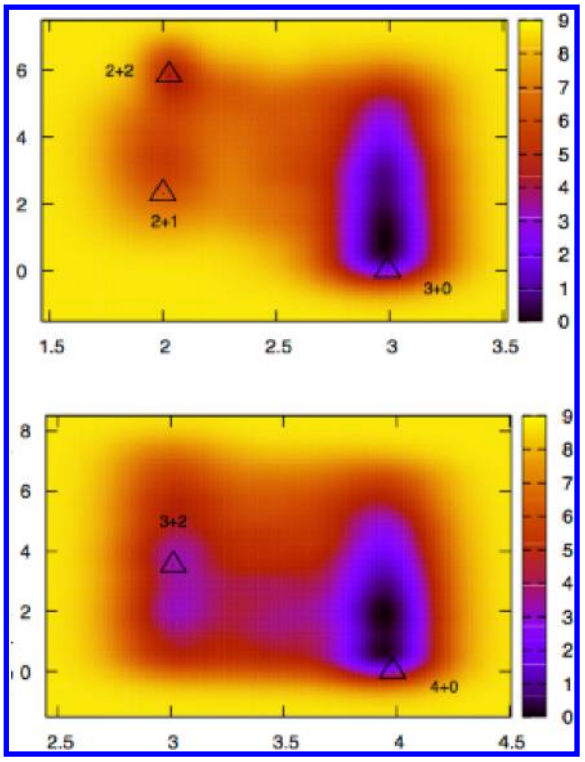

Figure 5. Free energy profiles extracted from biased metadynamics for $Li^+(H_2O)_3$ (top) and $Li^+(H_2O)_4$ (bottom). The energy scaling is on the right-hand side, in kcal/mol. The zero of free energy is taken at the value of the lowest energy conformer. Horizontal axis: coordination of Li^+ with respect to the water oxygen atoms (see expression 1). Vertical axis: dipole moment of the water cluster (Debye). Triangle symbols on the plots represent minima of the clusters.

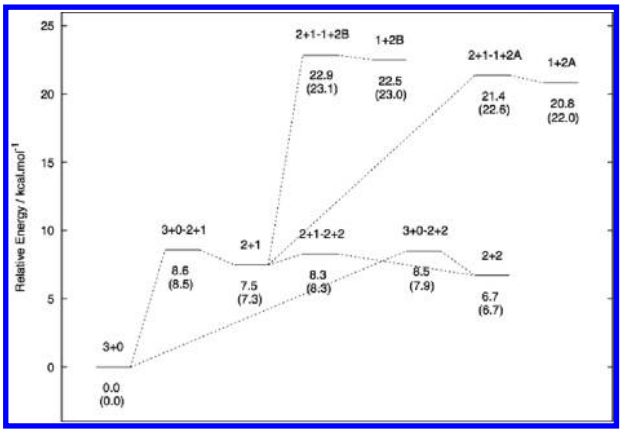

Figure 6. Schematic view of the potential energy surface of $Li^+(H_2O)_3$. Energies (in kcal/mol) are those from geometries optimized at the MP2 level, and the bracket energies are those from CP2K single point calculations.

low energy barriers of less than 1 kcal/mol are furthermore obtained between the higher energy conformers, i.e., 1+2B or 1+2A and conformer 2+1. The scheme in Figure 7 for $Li^+(H_2O)_4$ shows a somewhat simpler potential energy surface. Again, relatively low energy barriers are seen when connecting higher energy conformers (1+4 or 2+3) to lower energy ones, especially isomerization barriers down to conformer 3+2. The barrier between the two lower energy conformers 3+2 and 4+0 is ∼4 kcal/mol for 3+2 → 4+0 isomerization (∼5 kcal/mol for the reverse isomerization). These energetics are going to be

DOI: 10.1021/ct5008197
J. Chem. Theory Comput. 2015, 11, 871−883

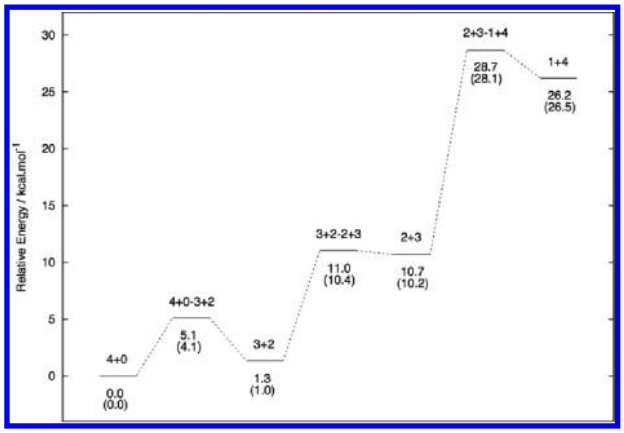

Figure 7. Schematic view of the potential energy surface of $Li^+(H_2O)_4$. Energies (in kcal/mol) are those from geometries optimized at the MP2 level, and the bracket energies are those from CP2K single point calculations.

useful when commenting on the results of the direct collision between the Li^+ cation and the $(H_2O)_{3,4}$ water cluster and formation of the associated $Li^+(H_2O)_{3,4}$ clusters with finite temperature DFT-MD simulations.

Nonstatistical Formation of $Li^+(H_2O)_{3,4}$ Isomers during the Collisions. Following the collisional protocol described in the Theoretical Methods section, the distribution of final conformers of $Li^+(H_2O)_3$ and $Li^+(H_2O)_4$ formed at the end of the 2 ps collisional processes are summarized in Figure 8, for cluster temperature of ~100 K. The ~100 K target temperature mirrors experimental conditions where $Li^+(H_2O)_nAr_m$ clusters are produced with at least one argon atom attached to the ion–water cluster. The plots in Figure 8 report the final conformer formed in relation with the initial impact angle and initial impact parameter of the collisions. See Figure 2 for the definitions of these two parameters. Plots on the left report results for direct formation of the final conformer, i.e., without conformational isomerization along the processes. Plots on the right report results for formation of the final conformer involving conformational isomerizations along the process, which are hereafter named cascade processes. See also Table 3 for a summary of results. An illustration of one collisional dynamics including conformational isomerization is presented in Figure 9.

Figure 8 clearly shows a nonstatistical distribution of conformers formed through the collisional process. The lowest energy conformers, namely, 3+0 of $Li^+(H_2O)_3$ and 4+0 of $Li^+(H_2O)_4$, are *predominantly* formed for an initial collisional impact angle lower than 45°, where the impact angle is measured from a vector, normal to the plane of the cyclic water trimer or tetramer (schemes in Figure 2). The direct formation of 3+0 is seen in a few instances for initial angles >45°. This occurs either when the water cluster rotates on the approach of the ion or when one hydrogen bond breaks and allows the ion to pass. The value of the initial collisional impact parameter has no influence. Analyses of the trajectories reveal that such a boundary for the initial collisional impact angle leads to a direct

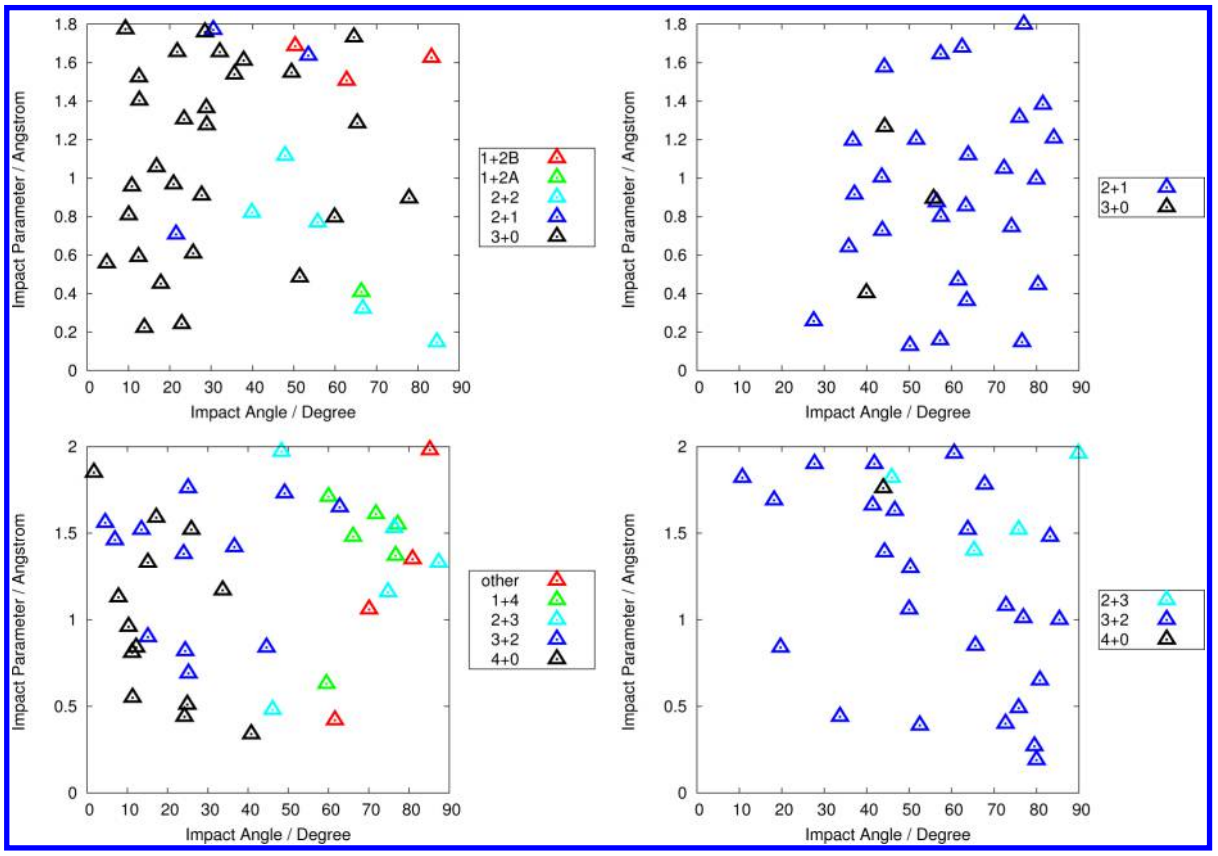

Figure 8. Representation of final isomers formed for $Li^+(H_2O)_3$ (top) and $Li^+(H_2O)_4$ (bottom) at the end of the 2 ps of 100 K DFT-MD collisional trajectories depending on the initial impact parameter and angle of collision, for direct (without conformation isomerization, left) and cascading (with conformational isomerization(s), right) formation processes. Colors are related to $Li^+(H_2O)_{3,4}$ isomers, ranked by increasing relative energies (from black (lowest) to red (higher energy)). See Figure 2 for schemes and definitions of 'impact parameter' and 'angle of collision' (theta).

DOI: 10.1021/ct5008197
J. Chem. Theory Comput. 2015, 11, 871–883

Table 3. Summary of the Collisional Processes from DFT-MD Trajectories

	total	direct	indirect processes
		$Li^+(H_2O)_3$	
3+0	31/70	28	(1×) 2+1 → 3+0
			(2×) 1+2B → 2+1 → 3+0
2+1	30/70	3	(27×) 1+2B → 2+1
2+2	5/70	5	-
1+2A	1/70	1	-
1+2B	3/70	3	-
$Li^+(H_2O)_4$			
4+0	14/70	13	(1×) 2+3 → 4+0
3+2	37/70	12	(13×) 2+3 → 3+2
			(12×) 1+4 → 2+3 → 3+2
2+3	9/70	5	(4×) 1+4 → 2+3
1+4	6/70	6	-
others	4/70		

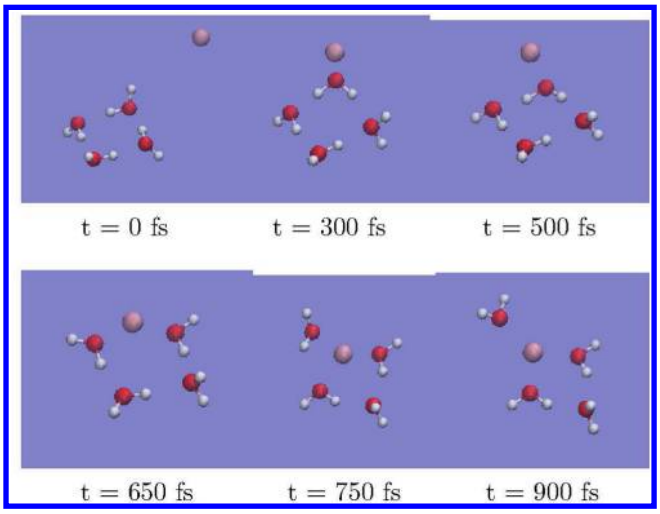

Figure 9. Snapshots extracted from a collisional trajectory showing the formation of the 3+2 conformer of $Li^+(H_2O)_{3,4}$ cluster.

insertion of the Li^+ into the water cluster, which naturally leads to the formation of the lowest energy conformers: this is obtained for 44% and 20% of the collisional trajectories of $Li^+(H_2O)_3$ and $Li^+(H_2O)_4$, respectively. Interestingly, the vast majority of the 3+0 isomer of $Li^+(H_2O)_3$ is formed through a direct process; see Table 3. The very minor indirect processes for the formation of isomer 3+0 show the following cascading isomerization processes 1+2B → 2+1 → 3+0 (twice) and 2+1 → 3+0 (once). These three trajectories correspond to an initial collisional impact angle close to the boundary of 45°. They furthermore show that the system has enough energy to overpass the 1.1 kcal/mol energy barrier separating 2+1 and 3+0 at the end of the collisional process (as well as the initial barrier 1+2B → 2+1 seen in one process, less than 1 kcal/mol of energy).

All other collisional trajectories lead to the formation of higher energy conformers: isomers 2+1 and 2+2 of $Li^+(H_2O)_3$ are respectively formed in 43% and 7% of the collisions. While isomer 2+2 is formed directly, isomer 2+1 is predominantly formed through cascading processes with the systematic isomerization cascade 1+2B → 2+1 (occurs 27 times over 30 trajectories leading to 2+1, see Table 3). This latter isomerization requires less than 1 kcal/mol of energy barrier to overcome.

For clusters formed with low temperature (100 K here), the picosecond time scale dynamics thus show that 44% of the collisions end up in the formation of the lowest energy isomer 3+0 of $Li^+(H_2O)_3$ and 43% end up in the formation of the higher energy isomer 2+1. We have also obtained three trajectories where 2+1 isomerizes into 3+0 within this time scale, thus showing that once 2+1 is formed it has enough energy to pass over the barrier leading to the lowest energy isomer 3+0, even in a few ps. We thus anticipate that isomers 2+1 will systematically isomerize into 3+0 over slightly longer time scales, thus leading to 100% formation of isomer 3+0. We will come back to this point with RRKM calculations.

In the case of $Li^+(H_2O)_4$, 53% of the collisional trajectories end up into 3+2 isomer over 1−2 ps time scale. Interestingly, only a minority of trajectories results in the direct formation of 3+2 conformer (32%), while the vast majority of the trajectories (68%) result in the formation of 3+2 through the cascading isomerization processes. Depending on the collisional initial impact angle, 3+2 can be formed via the 1+4 → 2+3 → 3+2 isomerization sequence (collisional initial angles above 45°) or via the 2+3 → 3+2 sequence (without any influence of the collisional initial angle). These isomerization processes are extremely fast over the 1−2 ps trajectories. The highest energy barrier for these cascading processes is 2.5 kcal/mol (1+4 → 2+3) and is systematically overcome at the start of the collisional process. Strikingly, the direct and cascading formation of the 3+2 conformer occurs for all ranges of initial angles and impact parameters of the collisions. A few of the trajectories also end up in much higher energy conformers, 1+4 and 2+3 at the end of the trajectories, but they will certainly evolve toward isomer 3+2 over a longer time-scale (in a few picoseconds). Indeed, as seen with the 25 trajectories associated with the cascading formation of isomer 3+2, the cluster has enough energy to overpass the barriers of 1+4 → 2+3 → 3+2 pathways during the ∼2 ps collisional process. One can thus anticipate that the 15 trajectories that end up as isomers 1+4 and 2+3 after 1−2 ps time scale will ultimately lead to isomer 3+2 in a few more picoseconds.

Overall we thus expect 52 trajectories leading to isomer 3+2 and, therefore, 74% of the collisions leading to the formation of the higher energy isomer 3+2, after a few picoseconds. An energy barrier of 3.8 kcal/mol remains to be overcome in order to lead to the lowest energy isomer 4+0. The lowest energy isomer 4+0 is formed only over 20% of the collisions, predominantly via the direct insertion of Li^+ within the water tetramer (13 trajectories over 14), and *only* for collisional impact angles less than 45°. The single trajectory showing the cascading formation of isomer 4+0 follows the pathway 2+3 → 4+0 and arises from an initial collisional angle at the 45° boundary.

Temperature Effects on the Trapping of Higher Energy Conformers. At cluster temperature of ∼100 K and at the end of 2 ps collisional trajectories, the higher energy conformer 3+2 of $Li^+(H_2O)_4$ is thus formed by a large majority, while the total population of the higher energy conformers 2+1 and 2+2 of $Li^+(H_2O)_3$ is slightly larger than the lowest energy conformer, 3+0. The influence of the temperature during the collisional process was investigated by redoing a few simulations at lower (50 K) and higher (300 K) temperatures. These temperatures respectively mirror experimental conditions where the $Li^+(H_2O)_n$ clusters are formed with at least one argon atom attached to the ion−water cluster (50 K) and without argon atom attached (300 K). Hence, two simulations

DOI: 10.1021/ct5008197
J. Chem. Theory Comput. 2015, 11, 871−883

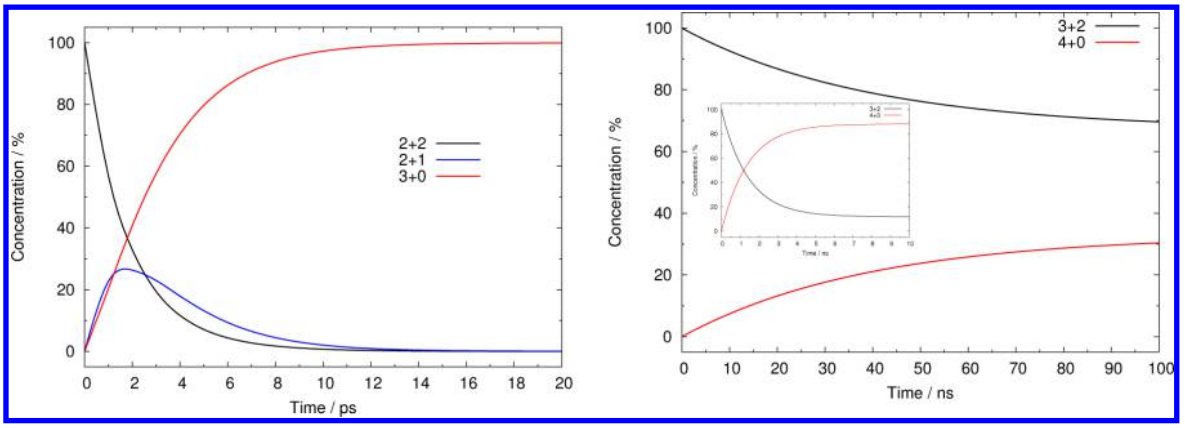

Figure 10. RRKM evolution of the population of $Li^+(H_2O)_3$ (left) and $Li^+(H_2O)_4$ (right) isomers. Initial populations: 2+2 (100%), 2+1, and 3+0 (0%) [left] and 3+2 (100%) and 4+0 (0%) [right]. Calculations performed with the MP2 PES. Temperature of cluster set to 60 K, apart for the inset (right) at 76 K.

leading to the formation of the 4+0 lowest energy conformer at 100 K were reinvestigated at these two supplementary temperatures, starting from the same geometry (directions kept) but modifying the initial velocities according to the desired temperature. Both trajectories now lead to higher energy conformers when they are run at 50 K (2+3 conformer in one case and 3+2 otherwise), whereas the 300 K collisional trajectories lead to the lowest energy conformer 4+0. Similar outcomes are obtained when reinvestigating collisional trajectories leading to the 3+2 conformer at 100 K. At the lower temperature of 50 K, the higher-energy conformers 1+4 and 2+3 are now formed. At 300 K, 3+2 conformer can still be formed, but some trajectories also lead to the formation of the 4+0 conformer.

Collisional trajectories thus show that when the temperature is low enough, i.e., when the internal energy of $Li^+(H_2O)_n$ is low, there is insufficient energy within the system to overcome the energy barriers between high energy conformers along the isomerization processes, whereas when the internal energy increases these barriers can be overcome over short periods of time. Higher energy collisions tend to more systematically lead to the formation of the lowest energy conformer of $Li^+(H_2O)_n$, while the reverse occurs for lower energy collisions; they lead to the formation of higher energy conformers. Such clusters have insufficient internal energy for overpassing the barrier(s) that would ultimately lead to the formation of lower energy conformers through subsequent cascading processes.

What Have We Learned from Picosecond DFT-MD Trajectories? DFT-MD trajectories have been accumulated over a rather short period of 2 ps, but they already provided a wealth of information on the *nonstatistical mechanisms* at the heart of the collisional processes for the formation of the $Li^+(H_2O)_{3,4}$ clusters and on isomerization processes. The collisional dynamics taking into account the argon evaporation process and its associated internal energy cooling process, at 100 K, clearly show that they are leading to (1) the formation of the lowest energy isomer (3+0) in the case of $Li^+(H_2O)_3$. The (2+1) isomer, formed in roughly equal number, has enough internal energy to evolve toward (3+0), which we already saw occurring during some of the 1−2 ps DFT-MD dynamics; and (2) to the formation of the higher energy 3+2 conformer of the $Li^+(H_2O)_4$ cluster by a vast majority (74%). The lowest energy conformer 4+0 is also formed, but to a much lower extent of 20%.

One pivotal conclusion is that the *nonstatistical* behaviors for the initial step(s) in the formation of the $Li^+(H_2O)_{3,4}$ clusters could not be generated by a *statistical theory* such as RRKM. This demonstrates the impact of theories to be used for the early steps of formation of the clusters. Once this initial picosecond stage has been attained, one can use the RRKM formalism in order to assess the longer microseconds stage of conformational isomerization. RRKM has the benefit that the *ab initio* representation of the potential energy surface is maintained.

Conformational Isomerization over the Microsecond Time-Scale. RRKM results are summarized in Figure 10 for $Li^+(H_2O)_3$ (left) and $Li^+(H_2O)_4$ (right). RRKM calculations have been done at different temperatures of the clusters, mirroring the temperature effect seen in the DFT-MD collisions. As the two series of clusters have different sizes, we use temperature as a measurement scale in our discussions below instead of internal energies. The two figures respectively report the evolution with time of the population of isomers 2+2, 2+1, and 3+0 in the case of $Li^+(H_2O)_3$ and of isomers 3+2 and 4+0 in the case of $Li^+(H_2O)_4$, for a given initial T = 60 K of isomer 2+2 ($Li^+(H_2O)_3$) and 3+2 ($Li^+(H_2O)_4$).

Once $Li^+(H_2O)_3$ cluster has a temperature of ∼60 K, isomerization processes between 2+2, 2+1, and 3+0 occur, ultimately leading to 100% of isomer 3+0 formed in less than 10 ps. This time is reduced to ∼4 ps for a cluster temperature of ∼100 K. These short time scales indeed correspond to the isomerization processes already observed during the DFT-MD collisional trajectories. These calculations confirm that the lowest energy isomer 3+0 of $Li^+(H_2O)_3$ will be the dominant conformer over the microsecond time scale of the experiment, for temperatures 60−100 K. Higher temperatures will obviously favor even more the formation of 3+0.

In the case of $Li^+(H_2O)_4$, a minimal cluster temperature of 60 K is necessary for isomerization from isomer 3+2 to the lowest energy isomer 4+0. The 3+2 → 4+0 isomerization occurs at a slow rate, without a reversal of the two populations: one thus finds 67% of the initial population of isomer 3+2 remaining at the end of the 100 μs time scale. When the cluster temperature is increased to 76 K, a much faster 3+2 → 4+0 isomerization occurs, with a reversal of populations over a nanosecond time-scale (inset in Figure 10). After 10 ns, a plateau is reached, and one finds that approximately 90% of the initial population of 3+2 has isomerized into 4+0. A 100%

DOI: 10.1021/ct5008197
J. Chem. Theory Comput. 2015, 11, 871−883

isomerization is obtained for temperature beyond 100 K, within a few nanoseconds.

Of course, these theoretical results primarily depend on the energy barrier between 3+2 and 4+0 isomers (and to a lesser extent on the energy difference between the two isomers), as well as the temperature of the clusters. Energetics obtained at the MP2 level have an accuracy of 1−2 kcal/mol at the best, even for this rather high level electronic representation. We have thus redone the RRKM calculations taking into account a modulation of the energy of the transition state between 3+2 and 4+0 by ±2 kcal/mol. Not surprisingly, the 3+2 → 4+0 isomerization thus takes place at a lower temperature when the energy barrier is reduced. Hence, 100% of the 3+2 population isomerizes into 4+0 once the cluster temperature is ≥30 K. If the 3+2 → 4+0 transition state energy is increased instead, a temperature of 106 K is needed for the population of the 4+0 configuration to exceed that for the 3+2 within 30 ns. Only 17% of the initial 3+2 population remains after 100 microseconds. Vibrational anharmonicity in the noncovalent modes does not appear to have an effect. This was checked by varying the frequencies of these modes by 10%.

Estimation of Cluster Temperature Formed in the Experiment. Can we use our combined DFT-MD trajectory collisions and statistical evolution of isomeric populations to provide a robust estimate of the cluster temperature formed in the experiment? Temperatures have been experimentally estimated in the range 50−150 K for argonated clusters,[23,24] and the IRPD experiments using the argon loss channel show that isomer 3+2 is the one predominantly probed in the experiment.[16] Our combined theoretical approaches thus suggest a temperature of the $Li^+(H_2O)_4$ clusters in the range 60−100 K. At these temperatures the RRKM theory estimates that only 33% of the initial 3+2 isomeric population has evolved into the lowest energy conformer 4+0, thus keeping a large majority of 3+2 isomers to be probed by the IR photon and subsequent photon dissociation. Beyond that temperature range, 100% of the 3+2 population isomerizes into 4+0. Note furthermore that collisions achieved at the lower temperature of 50 K showed that isomer 3+2 was more systematically formed, even for the collisional trajectories that led to the lowest energy isomer 4+0 at the higher temperature of 100 K. Within this temperature range, $Li^+(H_2O)_3$ already fully isomerizes into the lowest energy conformer 3+0.

■ CONCLUSIONS AND PERSPECTIVES

In the range ∼60−100 K, we have demonstrated that the lowest energy isomer 3+0 of $Li^+(H_2O)_3$ is systematically formed through collision and evaporative cooling, while a higher energy conformer 3+2 is predominantly formed for $Li^+(H_2O)_4$ together with a smaller population of the lowest energy isomer 4+0. These conclusions are obtained by 2 ps time-scale DFT-MD direct dynamics of the collision between the cation and the water clusters, including evaporative cooling of the clusters as they form, combined with RRKM isomerization processes over the microsecond time-scale. The formation of the clusters by collision has been shown to be nonstatistical, thus requiring direct dynamics of the collision to be modeled. Clusters form by both direct and cascade processes. The temperature, collision impact parameter, and collision angle with respect to the plane of oxygens in the preformed cyclic water species influence the dynamical formation pathway (direct vs cascade) and the resulting conformation distribution. When the lowest energy isomers are not formed by a direct process, cascade(s) of isomerization(s) from high to lower energy isomers take place, where temperature plays a crucial role in the potential trapping of high energy conformers. The lower the temperature the higher the probability of trapping high energy conformers: at low internal energy, clusters do not have enough energy for overcoming the barriers to isomerization and cannot proceed further along the path to lower energy configurations. On the contrary, we showed that the lower energy conformers of $Li^+(H_2O)_{3,4}$ are systematically formed for cluster temperatures above 100 K, corresponding to the results observed for nonargonated $Li^+(H_2O)_{3,4}$ clusters in the experiments.

The theoretical calculations presented here have provided a microscopic understanding for the formation of $Li^+(H_2O)_{3,4}$ clusters as they occur in our experimental setup. IRPD experiments and the combined dynamic−kinetic theoretical approaches developed here thus provide a synergetic tool to map potential energy surfaces of ionic clusters. Not only the lowest energy conformer but also higher energy conformers can be characterized, with estimates of energy barriers to isomerization and pathways for isomerization. The synergy should work along the following lines, with forward and backward interplay between experiments and theoretical calculations:

- Direct dynamics of collisions combined with RRKM evolution of populations provide a roadmap for the IRPD experiments. They indeed give a nonstatistical distribution of conformers formed from the initial collision and show how that distribution evolves on the microsecond time scale, taking into account temperature and entropic effects, together with dynamical effects. Identification of the high energy conformers possibly trapped along the cascade processes is obtained, including knowledge of cluster temperatures needed for their trapping. Note that knowledge of energy barriers is not necessary for the dynamical step as the direct modeling of the collisional process and cluster formation does not need this information. In fact, the dynamics provides an a posteriori knowledge of these barriers through the analyses of conformers formed along the collisional processes and the knowledge of the trapped conformers, in relation with temperature of the clusters.
- This in turn directs the IRPD experiments to be performed by giving the knowledge of fragmentation channels worth exploring, in direct relation with cluster temperatures. The choice of evaporative species, water from nonargonated species, or argon from argonated cluster ions indeed affects the final temperature of the cluster ion and the amount of energy available to overcome conformational barriers.
- Depending on the loss channel, spectroscopic signatures of lowest/higher energy conformers will be characterized. This provides a *direct experimental measure* of the minima on the PES, i.e., low and higher energy conformers. Experimental and dynamical theoretical spectra including anharmonic vibrational effects[18,52] can furthermore be compared at that stage. This spectroscopic comparison is presented in ref 53 for the $Li^+(H_2O)_{3,4}$ clusters of interest here.
- The experiments in turn validate/invalidate the theoretical map from step 1 above and thus possibly help refine the level of theoretical representation and time-scales needed in the theoretical calculations.

DOI: 10.1021/ct5008197
J. Chem. Theory Comput. 2015, 11, 871−883

From the simulations and supporting experiments shown here, two more general observations can be made concerning the requirements to reach the global minimum on the potential energy surface. First, in the absence of a direct path, an indirect or cascade process/pathway must lead to the global minimum. In the $Li^+(H_2O)_n$ ionic systems, this was guaranteed based on the size and nature of the systems. Second, there must be sufficient energy to overcome conformational barriers on the time scale of the experiment. Otherwise, kinetically trapped, higher energy conformers will remain within the ensemble unable to progress any further toward the global minimum.

We intend to extend these studies to the PES mapping of M^+(biomolecule)$(H_2O)_n$ ionic clusters,[18,54] which possess greater complexity, higher barriers, and deeper and more numerous minima.

AUTHOR INFORMATION

Corresponding Authors

*(J.M.L.) E-mail: j-lisy@illinois.edu.

*(M.-P.G.) E-mail: mgaigeot@univ-evry.fr.

Notes

The authors declare no competing financial interest.

ACKNOWLEDGMENTS

National Science Foundation under Grant Nos. CHE-0748874 and CRIF 05-41659 is acknowledged. Computational resources were provided by support from HPC resources from GENCI-France [IDRIS] (Grant 2012-2014 [072484]) and from the United States National Science NICS/XSEDE under Grant TG-CHE120083. J.M.L. and M.-P.G. acknowledge the United States National Science Foundation (CHE-1124821) and the French ANR SPIONCLUS, respectively, for research support through the International Collaboration in Chemistry Program (ANR-NSF). J.M.L. also acknowledges that this material is based on work supported while serving at the National Science Foundation. J.P. Beck and P. Lopez-Tarifa are acknowledged for stimulating discussions.

REFERENCES

(1) Simons, J. P. *Mol. Phys.* **2009**, *107*, 2435.
(2) Rizzo, T.; Stearns, J.; Boyarkin, O. *Int. Rev. Phys. Chem.* **2009**, *28*, 481.
(3) Polfer, N.; Oomens, J. *Mass Spectrom. Rev.* **2009**, *28*, 468.
(4) Polfer, N. *Chem. Soc. Rev.* **2011**, *40*, 2211.
(5) Stedwell, C.; Galindo, J.; Roitberg, A.; Polfer, N. *Annu. Rev. Anal. Chem.* **2013**, *6*, 267.
(6) Mosley, J.; Young, J.; Duncan, M. *J. Chem. Phys.* **2014**, *141*, 024306.
(7) Forck, R.; Dieterich, J.; Pradzynski, C.; Huchting, A.; Mata, R.; Zeuch, T. *Phys. Chem. Chem. Phys.* **2012**, *14*, 9054.
(8) Yang, B.; Rodgers, M. *Phys. Chem. Chem. Phys.* **2014**, *16*, 16110.
(9) Yoneya, M.; Tsuzuki, S.; Yamaguchi, T.; Sato, S.; Fujita, M. *ACS Nano* **2014**, *8*, 1290.
(10) Held, M.; Noé, F. *Eur. J. Cell. Biol.* **2012**, *91*, 357.
(11) Castellanos, M.; Perez, R.; Carrillo, P.; de Pablo, P.; Mateu, M. *Biol. J.* **2012**, *102*, 2615.
(12) Papadopoulos, G.; Svendsen, A.; Boyarkin, O.; Rizzo, T. *J. Am. Soc. Mass Spectrom.* **2012**, *23*, 1173.
(13) Silveira, J.; Fort, K.; Kim, D.; Servage, K.; Pierson, N.; Clemmer, D.; Russell, D. *J. Am. Chem. Soc.* **2013**, *135*, 19147.
(14) Fort, K.; Silveira, J.; Pierson, N.; Servage, K.; Clemmer, D.; Russell, D. *J. Phys. Chem. B* **2014**, *118*, 14336.
(15) Zehnacker, A. *Int. Rev. Phys. Chem.* **2014**, *33*, 151.
(16) Rodriguez, O., Jr.; Lisy, J. M. *J. Phys. Chem. Lett.* **2011**, *2*, 1444.
(17) Rodriguez, J. D.; Lisy, J. *Int. J. Mass Spectrom.* **2009**, *283*, 135.
(18) Brites, V.; Nicely, A.; Sieffert, N.; Gaigeot, M.-P.; Lisy, J. *Phys. Chem. Chem. Phys.* **2014**, *16*, 13086.
(19) Dian, B.; Longarte, A.; Zwier, T. *Science* **2002**, *296*, 2369.
(20) Dian, B.; Clarkson, J.; Zwier, T. *Science* **2004**, *296*, 1169.
(21) Leavitt, C.; Wolk, A.; Fournier, J.; Kamrath, M.; Garand, E.; Stipdonk, M. V.; Johnson, M. A. *J. Phys. Chem. Lett.* **2012**, *3*, 1099.
(22) Wales, D. *Energy Landscapes With Applications to Clusters, Biomolecules and Glasses*; Cambridge University Press: 2003.
(23) Miller, D.; Lisy, J. *J. Am. Chem. Soc.* **2008**, *130*, 15381.
(24) Miller, D.; Lisy, J. *J. Am. Chem. Soc.* **2008**, *130*, 15393.
(25) Vaden, T. D.; Weinheimer, C.; Lisy, J. *J. Chem. Phys.* **2004**, *121*, 3102.
(26) Munoz, F.; Rogan, J.; Valdivia, J.; Varas, A.; Kiwi, M. *Physica B* **2013**, *427*, 76.
(27) Frisch, M. J.; Trucks, G. W.; Schlegel, H. B.; Scuseria, G. E.; Robb, M. A.; Cheeseman, J. R.; Scalmani, G.; Barone, V.; Mennucci, B.; Petersson, G. A.; Nakatsuji, H.; Caricato, M.; Li, X.; Hratchian, H. P.; Izmaylov, A. F.; Bloino, J.; Zheng, G.; Sonnenberg, J. L.; Hada, M.; Ehara, M.; Toyota, K.; Fukuda, R.; Hasegawa, J.; Ishida, M.; Nakajima, T.; Honda, Y.; Kitao, O.; Nakai, H.; Vreven, T.; Montgomery, J. A., Jr.; Peralta, J. E.; Ogliaro, F.; Bearpark, M.; Heyd, J. J.; Brothers, E.; Kudin, K. N.; Staroverov, V. N.; Kobayashi, R.; Normand, J.; Raghavachari, K.; Rendell, A.; Burant, J. C.; Iyengar, S. S.; Tomasi, J.; Cossi, M.; Rega, N.; Millam, J. M.; Klene, M.; Knox, J. E.; Cross, J. B.; Bakken, V.; Adamo, C.; Jaramillo, J.; Gomperts, R.; Stratmann, R. E.; Yazyev, O.; Austin, A. J.; Cammi, R.; Pomelli, C.; Ochterski, J. W.; Martin, R. L.; Morokuma, K.; Zakrzewski, V. G.; Voth, G. A.; Salvador, P.; Dannenberg, J. J.; Dapprich, S.; Daniels, A. D.; Farkas, O.; Foresman, J. B.; Ortiz, J. V.; Cioslowski, J.; Fox, D. J. *Gaussian 09*, revision C.01; Gaussian, Inc.: Wallingford, CT, 2009.
(28) Møller, C.; Plesset, M. *Phys. Rev. A* **1934**, *46*, 618.
(29) Dunning, T. H., Jr. *J. Chem. Phys.* **1989**, *90*, 1007.
(30) Prascher, B.; Woon, D.; Peterson, K.; Wilson, T. D. J. A. *Theor. Chem. Acc.* **2011**, *128*, 69.
(31) Pople, J.; Head-Gordon, M.; Raghavachari, K. *J. Chem. Phys.* **1987**, *87*, 5968.
(32) CP2K is freely available from http://www.cp2k.org/.
(33) VandeVondele, J.; Krack, M.; Mohamed, F.; Parrinello, M.; Chassaing, T.; Hutter, J. *Comput. Phys. Commun.* **2005**, *167*, 103.
(34) Becke, A. *Phys. Rev. A* **1988**, *38*, 3098.
(35) Lee, C.; Yang, W.; Parr, R. *Phys. Rev. B* **1988**, *37*, 785.
(36) Grimme, S. *J. Comput. Chem.* **2006**, *27*, 1787.
(37) Goedecker, S.; Teter, M.; Hutter, J. *Phys. Rev. B* **1996**, *54*, 1703.
(38) Krack, M. *Theor. Chem. Acc.* **2005**, *114*, 145.
(39) Martyna, G. J.; Tuckerman, M. E. *J. Chem. Phys.* **1999**, *110*, 2810.
(40) Laio, A.; Parrinello, M. *Proc. Natl. Acad. Sci. U. S. A.* **2002**, *99*, 12562.
(41) Ensing, B.; Laio, A.; Parrinello, M.; Klein, M. L. *J. Phys. Chem. B* **2005**, *109*, 6676.
(42) Jorgensen, W.; Chandrasekhar, J.; Madura, J.; Impey, R.; Klein, M. *J. Chem. Phys.* **1983**, *79*, 926.
(43) Hu, X.; Hase, W.; Pirraglia, T. *J. Comput. Chem.* **1991**, *12*, 1014.
(44) Hase, W.; Duchovic, R.; Hu, X.; Komornicki, A.; Lim, K.; Lu, D.-H.; Peslherbe, G.; Swamy, K.; Linde, S. V.; Varandas, A.; Wang, H.; Wolf, R. *QCPE Bull.* **1996**, *16*, 671.
(45) Martin-Somer, A.; Yanez, M.; Gaigeot, M.; Spezia, R. *J. Phys. Chem. A* **2014**, *118*, 10882.
(46) Spezia, R.; Cimas, A.; Gaigeot, M.; Salpin, J.-Y.; Song, K.; Hase, W. H. *Phys. Chem. Chem. Phys.* **2012**, *14*, 11724.
(47) Cabarcos, O.; Lisy, J. *Chem. Phys. Lett.* **1996**, *257*, 265.
(48) Baer, T.; Hase, W. *Unimolecular Reaction Dynamics Theory and Experiments*; Oxford University Press: 1996.
(49) Robinson, P.; Holbrook, K. *Unimolecular reactions*; Wiley-Interscience: London, New York, 1972.
(50) Forst, W. *Theory of Unimolecular Reactions*; Academic: New York, 1973.
(51) Miller, W. *J. Am. Chem. Soc.* **1979**, *101*, 6810.
(52) Gaigeot, M. P. *Phys. Chem. Chem. Phys.* **2010**, *12*, 3336.

DOI: 10.1021/ct5008197
J. Chem. Theory Comput. 2015, 11, 871−883

(53) Brites, V.; Lisy, J.; Gaigeot, M. *J. Phys. Chem. A* **2015**, DOI: 10.1021/jp508699m.
(54) Beck, J.; Gaigeot, M.-P.; Lisy, J. *Phys. Chem. Chem. Phys.* **2013**, *15*, 16736.

DOI: 10.1021/ct5008197
J. Chem. Theory Comput. 2015, 11, 871−883